Biophysical Journal
Article

Biophysical Society

Measurement of the specific and non-specific binding energies of Mg^{2+} to RNA

A. Martinez-Monge,[1] Isabel Pastor,[1,5] Carlos Bustamante,[2,3,4] Maria Manosas,[1,5,*] and Felix Ritort[1,5,*]
[1]Small Biosystems Lab, Departament de Física de la Matèria Condensada, Facultat de Física, Universitat de Barcelona, Carrer de Martí i Franquès, 1, 08028 Barcelona, Spain; [2]Departments of Chemistry, Physics and Molecular and Cell Biology, University of California Berkeley, Berkeley, California; [3]Howard Hughes Medical Institute University of California Berkeley, Berkeley, California; [4]Kavli Energy Nanosciences Institute, University of California Berkeley, Berkeley, California; and [5]Institut de Nanociència i Nanotecnologia (IN2UB), Universitat de Barcelona, 08028 Barcelona, Spain

ABSTRACT Determining the non-specific and specific electrostatic contributions of magnesium binding to RNA is a challenging problem. We introduce a single-molecule method based on measuring the folding energy of a native RNA in magnesium and at its equivalent sodium concentration. The latter is defined so that the folding energy in sodium equals the non-specific electrostatic contribution in magnesium. The sodium equivalent can be estimated according to the empirical 100/1 rule (1 M NaCl is equivalent to 10 mM $MgCl_2$), which is a good approximation for most RNAs. The method is applied to an RNA three-way junction (3WJ) that contains specific Mg^{2+} binding sites and misfolds into a double hairpin structure without binding sites. We mechanically pull the RNA with optical tweezers and use fluctuation theorems to determine the folding energies of the native and misfolded structures in magnesium (10 mM $MgCl_2$) and at the equivalent sodium condition (1 M NaCl). While the free energies of the misfolded structure are equal in magnesium and sodium, they are not for the native structure, the difference being due to the specific binding energy of magnesium to the 3WJ, which equals $\Delta G \simeq 10$ kcal/mol. Besides stabilizing the 3WJ, Mg^{2+} also kinetically rescues it from the misfolded structure over timescales of tens of seconds in a force-dependent manner. The method should generally be applicable to determine the specific binding energies of divalent cations to other tertiary RNAs.

SIGNIFICANCE Magnesium ions play an essential role in RNA folding. On the one hand, the diffusive ion cloud screens the negative charges of the RNA backbone. On the other hand, magnesium ions can specifically bind to RNA sites, bringing together distal bases along the RNA backbone forming tertiary contacts. The knowledge of the non-specific and specific stabilizing energy contributions is essential for RNA folding and the formation of RNA-ligand complexes. We have developed a new experimental method based on single-molecule force spectroscopy to measure and separate the specific and non-specific contributions of Mg^{2+} to tertiary RNA stability. The methodology is applied to a ribosomal RNA three-way junction to which magnesium specifically binds, inducing a structural rearrangement.

INTRODUCTION

Electrostatic forces are crucial interactions in the regulation of biomolecular reactions inside the cell. Dissociated ions control the structure of charged biopolymers and their binding strength to ligands [1]. Nucleic acids are among the most densely charged polymers in nature [2]. In their double-stranded form, phosphate groups confer a high-density charge of 2 e^- per $\simeq$ 3Å, the repulsive force per base pair in solution being on the order of piconewtons. Such repulsion is counterbalanced by hydrogen bonding and base stacking that stabilize the double helix. Metal ions interact with nucleic acids non-specifically or diffusively by screening the negatively charged phosphate's backbone. They can also bind specifically to tertiary sites, either by tight binding to phosphates and sugars of the RNA backbone or forming coordination bonds directly or through the ion's hydration shell with charged groups of the different nucleic acid bases [3–5]. Although non-specific electrostatic interactions can be described using generalized activity theories of electrolytes (mean-field approaches such as the extended Debye-Hückel, Guoy-Chapman, Poisson-Boltzmann, the tight-binding ion model [6], the DLVO theory [7], and simulations [8]), much less is known about the specific interactions of metal ions binding to DNA and RNA structures [9]. Upon binding to some structural motifs, metal ions can induce conformational

*Correspondence: ritort@ub.edu or mmanosas@ub.edu
Editor: Mark Williams.
https://doi.org/10.1016/j.bpj.2022.07.020

changes similar, for example, to the action of riboswitches that regulate gene expression.

Divalent ions, such as magnesium, play a major role in stabilizing RNA structures by producing environments with unusually strong interactions [4,10–13] facilitating RNA folding [14]. Magnesium is also essential in cleavage reactions of autocatalytic RNAs [15,16] and the recently discovered interconversion between multiple folds in RNAs with enzymatic activity [17–19]. The two positive charges of Mg^{2+} interact with the polarized hydroxyl group of the ribose, bringing together distant nucleotides in the RNA chain facilitating tertiary structure formation. The specific and non-specific stabilizing energy contributions are known to be approximately additive [20,21]. However, the contribution of specifically binding magnesium ions to the formation of RNA structures is poorly known, at least compared with the (diffusive) non-specific electrostatic screening effects [22–24].

Here we introduce a new experimental method based on single-RNA mechanical unzipping experiments to separate the specific and non-specific electrostatic interactions of RNA structures in magnesium (Fig. 1). The idea is to extract from the unzipping data the folding free energy ΔG of the native (N) structure in magnesium at concentration $[Mg^{2+}]$ and at its equivalent sodium concentration $[Na^+]_{equiv}$. The latter is defined as the sodium concentration at which the stabilizing free energy contribution in N by the (non-specific) diffusive cloud of ions equals that at $[Mg^{2+}]$. $[Na^+]_{equiv}$ can be estimated by using the 1/100 empirical rule, which states that $[Na^+]_{equiv}$ is about 100-fold the value of $[Mg^{2+}]$ [24–28]. Alternatively, one can use a misfolded (M) structure, which lacks the magnesium binding site, as a calibration structure for the non-specific binding contribution. The equivalent amount of sodium, $[Na^+]_{equiv}$, contributing to the non-specific stabilization of RNA in magnesium, can then be determined as $\Delta G_{MU}([Na^+]_{equiv}) = \Delta G_{MU}([Mg^{2+}])$. This might be useful for the case of metallic ions (e.g., iron, manganese, cobalt, zinc, and other polycations) where an equivalence salt rule is unknown.

The procedure to extract the specific magnesium binding contribution is illustrated in Fig. 1 *A*. From pulling data, we measure the free energy of formation of a folded structure F (such as the native), first in magnesium ($\Delta G_{FU}([Mg^{2+}])$, Fig. 1 *A*, left), then in sodium ($\Delta G_{FU}([Na^+])$, Fig. 1 *A*, right). The calibration misfolded structure M is used to determine $[Na^+]_{equiv}$ at which the folding energy of M equals that in $[Mg^{2+}]$, $\Delta G_{MU}([Mg^{2+}]) = \Delta G_{MU}([Na^+]_{equiv})$. The folding free energy of F measured at the sodium equivalent, $\Delta G_{FU}\left([Na^+]_{equiv}\right)$, gives the non-specific energy contribution to the folding free energy of F in magnesium,

$$\Delta G_{FU}^{nsp,Mg^{2+}} = \Delta G_{FU}\left([Na^+]_{equiv}\right) \tag{1}$$

By subtracting Eq. 1 to the full free energy of F in magnesium, $\Delta G_{FU}([Mg^{2+}])$, we get the specific contribution of magnesium to the folding free energy of F (Fig. 1 *A*, right). This leads to our main definition,

$$\begin{aligned}\Delta G_{FU}^{sp,Mg^{2+}} &= \Delta G_{FU}\left([Mg^{2+}]\right) - \Delta G_{FU}^{nsp,Mg^{2+}} = \\ &= \Delta G_{FU}\left([Mg^{2+}]\right) - \Delta G_{FU}\left([Na^+]_{equiv}\right)\end{aligned} \tag{2}$$

Eq. 2 holds for all folded structures F, the various ΔG terms changing for different F structures of the same primary sequence. In the specific case F $\equiv$ M, $\Delta G_{MU}^{sp,Mg^{2+}} = 0$ by definition.

The applicability of the approach relies on two main assumptions. First, specific and non-specific magnesium

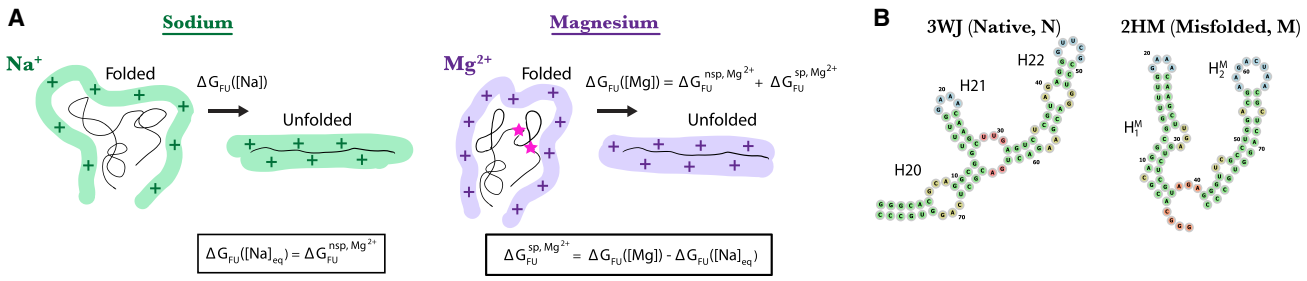

FIGURE 1 Schematics of the method and the RNA 3WJ. (*A*) The free energy of formation of a generic RNA structure (e.g., N or M), ΔG_{FU}, defined as the difference of free energy between folded (F) and unfolded (U) states, can be estimated from unzipping data. In magnesium, this free energy has contributions from specific Mg^{2+} binding, $\Delta G_{FU}^{sp,Mg^{2+}}$, and non-specific electrostatic screening, $\Delta G_{FU}^{nsp,Mg^{2+}}$ (right), whereas in sodium we assume no specific binding (left). The equivalent sodium concentration $[Na^+]_{equiv}$ is defined by Eq. 1 as the concentration at which the free energy of formation equals to the non-specific contribution in magnesium. The misfolded M that lacks the binding site can be used as a *calibration* structure for determining $[Na^+]_{equiv}$: $\Delta G_{MU}^{sp,Mg^{2+}} = 0$ and therefore $\Delta G_{MU}([Na^+]_{equiv}) = \Delta G_{MU}([Mg^{2+}])$. The free energy of formation of N in magnesium and at the sodium equivalent give the specific energy of Mg^{2+} binding, Eq. 2. (*B*) Secondary structures predicted by Mfold for the 3WJ RNA sequence: the native 3WJ (left) and misfolded 2HM (right) of energies 39 and 29 kcal/mol, respectively, at standard sodium conditions (298 K and 1 M NaCl). Colored bases indicate different motifs: Watson-Crick bp (green), outer loops (blue), inner loops (brown), and single-strand (red). To see this figure in color, go online.

contributions are additive. Second, for a given $[Mg^{2+}]$, the equivalent sodium concentration $[Na^+]_{equiv}$ gives the non-specific stabilization free energy of N due to the diffusive cloud of ions. Once $[Na^+]_{equiv}$ has been empirically determined, Eqs. 1 and 2 readily follow. These assumptions are supported by electrostatic theories that include correlations and fluctuations in the cloud of counterions [5,6,24,29]. Their validity is restricted to the diluted magnesium range where cooperative salt effects are negligible ($[Mg^{2+}] < 50$ mM) and competition effects with sodium are weak ($R = \sqrt{[Mg^{2+}]}/[Na^+] \gtrapprox 0.22$). Furthermore, previous melting studies of RNA oligos [24,26–28] and RNA unzipping [25] have shown that the equivalent sodium concentration $[Na^+]_{equiv}$ is approximately 100-fold that of magnesium. Recently, this result has been validated in RNA unzipping experiments at the level of individual base pair stacks [30]: the energy of the 10 distinct nearest-neighbor base pairs for a given magnesium concentration are equal to those in $77(\pm 49)$-fold sodium. However, there might be exceptions to this rule [31], so alternative approaches to determine $[Na^+]_{equiv}$ might be useful. One possibility is to use misfolded structures lacking specific magnesium binding sites as calibration structures, as we do in this work.

Here, we demonstrate the validity of the approach by investigating Mg^{2+} binding to an RNA three-way junction (hereafter referred to as RNA 3WJ) essential for the assembly of the small subunit of the bacterial ribosome [32] (Fig. 1 *B*, left). The junction belongs to the central domain of 16S rRNA from *Escherichia coli*, and is stabilized by binding to a small ribosomal protein S15, an important core and regulatory protein required for coordinated assembly of the bacterial ribosome [33–35]. The RNA-S15 complex facilitates subsequent binding of additional proteins (S6, S8, S11, S21) to form an essential platform for the formation of the 30S ribosomal subunit. This complex has been extensively studied for the case of *Thermus thermophilus*, *Bacillus stearothermophilus*, and *E. coli*. The solution structure of protein S15 has been determined by NMR [36] and the X-ray structure of the (S15, S6, S18)-rRNA ternary complex has been determined at 2.6 Å resolution [37]. The crystal structure of the whole 70S ribosome with nucleotide modifications has been also reported [38]. Recently, the structure of the 70S ribosome of *E. coli* has been determined with cryoelectron microscopy [39], the culmination of a long history of research activity in the structure of this ribosomal machine.

The S15-RNA complex is known to be conserved among bacteria through evolution [40]. The crystal structure of the *T. thermophilus* S15-3WJ RNA complex has been resolved with at 2.6 Å resolution [34]. The RNA 3WJ consists of three helices, H20, H21, and H22, and a highly conserved minimal binding site for S15 [34,41] (3WJ region, site 1 in Fig. 2). Magnesium is essential for S15 binding, by triggering a conformational transition of the RNA 3WJ that provides structural complementarity with S15 [42,43]. Without magnesium, S15 does not bind to the RNA, and helices H20, H21, and H22 form angles of 120° with each other. Mg^{2+} binding to the junction brings H22 toward H20 to approximately 60° angle and coaxially stacks H22 onto H21. This conformational change triggers binding of S15, demonstrating the critical role of Mg^{2+} in RNA-protein interactions. Some specific binding locations of Mg^{2+} have been determined (blue circles in Fig. 2), and a model of the interaction proposed [44,45]. In particular, three Mg^{2+} specifically bind close to the RNA junction (Fig. 2, blue circles at the lower part of the structure).

Despite the large number of studies, the specific binding energy of Mg^{2+} to the native 3WJ is unknown. Previous single-molecule studies have shown that the RNA 3WJ presents a misfolded (M) structure [46] in agreement with Mfold predictions [47]. M disrupts the binding site of the 3WJ forming two non-native hairpins (H_1^M and H_2^M) connected by three unpaired bases (Fig. 1 *B*, right), therefore neither Mg^{2+} ions nor S15 protein can bind specifically to the misfolded form (hereafter denoted by 2HM). The determination of the sodium equivalent, by either using the 1/100 rule or the misfolded structure, allows us to test our approach and determine, from Eqs. 1 and 2, the non-specific and specific free energy contributions of Mg^{2+} binding to the RNA 3WJ.

MATERIALS AND METHODS

Molecular construct and optical tweezers instrument

To synthesize the molecular construct with the RNA 3WJ, the sequence of 16S-3WJ DNA is cloned between EcoRI and HindIII restriction sites of pBR322 plasmid (purchased from Eurofins). The DNA template for the in vitro transcription was amplified with PCR. Besides the 16S-3WJ sequence, it contains 527 (handle A) and 599 (handle B) extra bases at each end, which are used to form DNA/RNA hybrid handles. After the in vitro transcription, labeled (biotin and digoxigenin) DNA handles that are complementary to the transcribed RNA template are hybridized at each flanking side of the 3WJ.

Pulling experiments were done using a counterpropagating dual-beam miniaturized optical tweezers instrument (see Ref. [48] for details). RNA-bead tethers are made by selectively binding biotin-labeled and digoxigenin-labeled handles to streptavidin (2.1 μm, Kisker Biotech) or anti-digoxigenin-coated beads (3.0–3.4 μm, Kisker Biotech). One bead is held by air suction on the tip of a glass micropipette; the other is optically trapped for force measurement from the deflected light detected by position-sensitive detectors (PSDs). The optical trap position is determined by diverting ~8% of each laser beam to a secondary PSD. Fig. 3 *A* shows the schematics of the experimental setup. Experiments were carried out at 25°C in magnesium buffer (10 mM $MgCl_2$, 50 mM NaCl, 10 mM Tris-HCl, pH = 7.5) and sodium buffer (1 M NaCl, 10 mM Tris-HCl, pH = 7.5).

Measurement protocols

We performed two kinds of experiments: pulling and hopping experiments [49]. In pulling experiments, the position of the optical trap λ is cyclically moved back and forth at a constant speed (e.g., 100 nm/s) between a

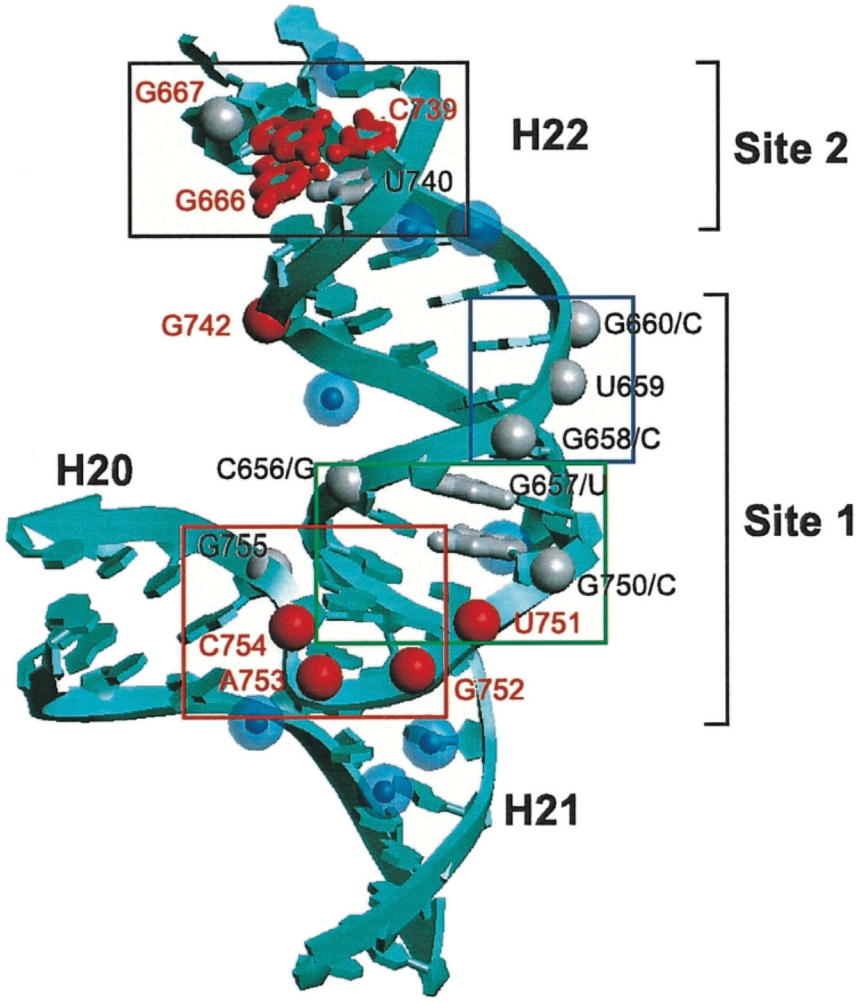

FIGURE 2 RNA 3WJ structure from *E. coli*. Crystal structure of the 57-nucleotide RNA corresponding to nucleotides 584–590/649–667/739–757 of *E. coli* rRNA complexed with the S15 protein from *Thermus thermophilus* [34]. Mg^{2+} ions are shown as blue circles. Three of them are located at the junction (lower part of the structure). Figure taken from [41]. To see this figure in color, go online.

maximum and a minimum force at two limit values of λ. At low forces, the RNA is found in a folded conformation (native or misfolded), whereas, at high forces, it is unfolded. Transitions between states can be identified as force jumps in the force-distance curves (FDCs). We also performed hopping experiments in the passive mode where the trap position (λ) is kept fixed, so the RNA explores states in equilibrium. In hopping experiments, the molecule executes transitions between states at different levels of force [50]. The force jumps observed in pulling and hopping experiments can be converted into number of released or absorbed nucleotides by using elastic polymer models for the single-stranded RNA (ssRNA) and RNA helices (Section 1 in Supporting material).

Free energy measurements with the extended fluctuation theorem

In thermodynamics, free energy differences ΔG are measured from the relation $\Delta G = W_{rev}$ where W_{rev} is the reversible work. In irreversible conditions, $\Delta G < W$, so the measured work W does not permit us to determine ΔG. In recent years, a new set of relations have been discovered that allow us to derive ΔG from irreversible work measurements. Key results are the Jarzynski equality [51] and the Crooks fluctuation theorem (CFT) [52]. The Jarzynski equality states that the exponential average of minus the work equals the exponential of minus the free energy difference, $-\ \Delta G$, both expressed in k_BT units,

$$\left\langle \exp\left(-\frac{W}{k_BT}\right)\right\rangle = \exp\left(-\frac{\Delta G}{k_BT}\right), \tag{3}$$

where $\langle \ldots \rangle$ stands for the average over trajectories. The convexity property of the exponential function leads to the second law inequality, $W \geq \Delta G$. CFT establishes a symmetry relation between the work delivered on a system in a nonequilibrium process and the work received by the system under time reversal of that process. In a typical nonequilibrium pulling experiment, the control parameter λ (i.e., the relative distance between the center of the optical trap and the tip of the micropipette) is cyclically moved back and forth between a minimum value (λ_0, corresponding to a low force) in which the molecule is folded and a maximum value (λ_1, corresponding to a high force) in which the molecule is unfolded. The unfolding process is identified with the forward protocol (F), whereas the folding process is identified with the reverse protocol (R). The CFT reads,

$$\frac{P_F(W)}{P_R(-W)} = \exp\left(\frac{W-\Delta G}{k_BT}\right), \tag{4}$$

where P_F and P_R are the work probability distributions in the F and R protocols and the minus sign in $P_R(-W)$ indicates that for the reverse process W changes sign. A corollary of the CFT is the Jarzynski equality, which can be obtained by rewriting Eq. 4 as $P_R(-W) = P_F(W)\exp(-(W-\Delta G)/k_BT)$, and

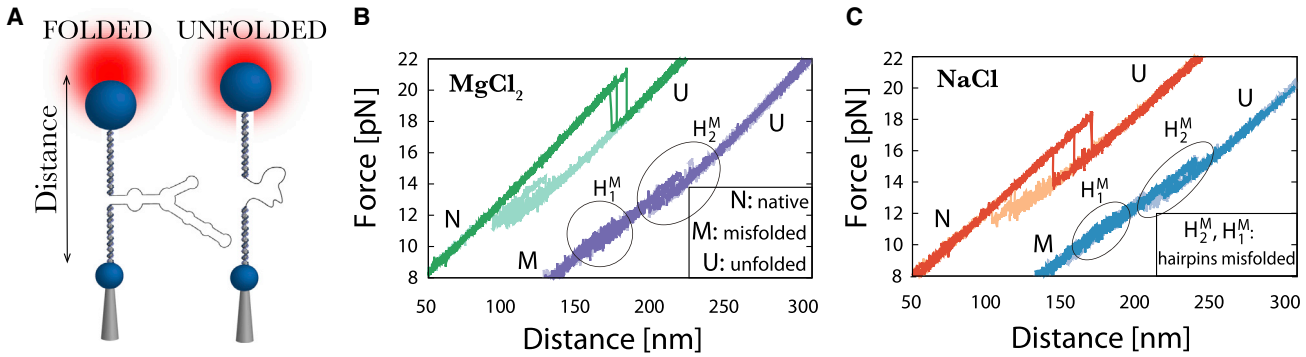

FIGURE 3 Dynamic force spectroscopy of the RNA 3WJ. (*A*) Optical tweezers experimental setup. The distance between the micropipette and the optical trap center is changed at a constant speed in a pulling protocol. FDCs for the N and M structures in 10 mM $MgCl_2$ (*B*) and 1 M NaCl (*C*) pulled at 100 nm/s at 298 K. At low forces, the molecule is folded in either the N or M structure and unfolds upon increasing the force. The folding and unfolding transitions are observed as force rips. To see this figure in color, go online.

integrating over W, $1 = \int dW P_R(-W) = \int dW P_F(W)\exp(-(W-\Delta G)/k_BT) = \langle \exp(-(W-\Delta G)/k_BT)\rangle$, from which Eq. 3 follows.

The Jarzynski equality and the CFT have been successfully applied to predict the free energy of molecular structures with a single native state [46,52]. An extension of the CFT (ECFT) permits us to recover the free energy of the native and misfolded states [53,54]. The ECFT reads:

$$\frac{\varphi_F^{A\to B}}{\varphi_R^{B\to A}}\frac{P_F^{A\to B}(W)}{P_R^{B\to A}(-W)} = \exp\left(\frac{W-\Delta G_{AB}}{k_BT}\right), \quad (5)$$

where A and B denote the initial and final states (which can be native, unfolded, or misfolded), and $\Delta G_{AB} = G_B(\lambda_1) - G_A(\lambda_0)$ is the free energy difference between state B at the final trap position λ_1 and state A at the initial trap position λ_0 along the pulling cycle; $P_F^{A\to B}(W)$ is the partial work distribution along the forward process ($A\to B$) restricted to those trajectories that start at A at λ_0 and end at B at λ_1. Conversely, $P_R^{B\to A}(W)$ is the partial work distribution along the reverse process ($B\to A$) restricted to those trajectories that start at B at λ_1 and end at A at λ_0. Finally, $\varphi_F^{A\to B}$ ($\varphi_R^{B\to A}$) is the fraction of trajectories starting in A (B) at λ_0 (λ_1) and ending in B (A) at λ_1 (λ_0). In the particular case of a single initial and final state, Eq. 5 leads to Eq. 4.

The free energy of folding of the 3WJ (N) and 2HM (M) relative to the unfolded (U) state, $\Delta G_{NU}, \Delta G_{MU}$, has been determined from pulling experiments by applying Eq. 5. FDCs are classified into two sets depending on whether they start (end) in N or M at λ_0 in the F (R) process (Fig. 3 *B* and *C*) from which $\varphi_R^{U\to N}$ and $\varphi_R^{U\to M}$ can be extracted. Note that in Eq. 5 $\varphi_F^{N\to U} = \varphi_F^{M\to U} = 1$ (all trajectories end in U along F), whereas $\varphi_R^{U\to N} + \varphi_R^{U\to M} = 1$ with $\varphi_R^{U\to N}, \varphi_R^{U\to M} < 1$; that is, refolding trajectories may end up either in N or M. We observe a misfolding probability of 5%–10%, giving $\varphi_R^{U\to M} \simeq 0.05 - 0.1, \varphi_R^{U\to N} \simeq 0.9 - 0.95$. Therefore, neglecting the term $\varphi_R^{U\to M}$ leads to a free energy underestimation of about $-k_BT\log(0.05) = 3\,k_BT$ for M. In contrast, for N the energy changes by less than $0.1\,k_BT$.

RESULTS

A molecular construct containing the RNA 3WJ was synthesized and pulled with laser optical tweezers (Fig. 3 *A*, Materials and methods). Pulling experiments were performed in a buffer containing 10 mM $MgCl_2$ and 50 mM NaCl (divalent condition). 2HM was used for sodium calibration as explained in the introduction. We verified that the monovalent condition $[Na^+]_{equiv} \simeq$ 1M is equivalent to the divalent one, in agreement with the most recent determination of the nearest-neighbour energy parameters from RNA unzipping experiments [30]. Force-distance curves (hereafter referred to as FDCs) in magnesium and at the equivalent sodium were recorded (Fig. 3 *B* and *C*). We observed two types of unfolding/folding patterns that we interpret as the unfolding of either the 3WJ or 2HM. Most of the time ($\simeq$90%), the unfolding curves display a single force jump event (leftmost curves in Fig. 3 *B* and *C*). The measured force jump is consistent with the release of the 77 bases forming the full 3WJ. For the conversion between nucleotides and force jump, we assumed the worm-like chain model for the ssRNA and a force-dependent trap stiffness [50,55] (Section 1 in Supporting material). Therefore, we relate this type of FDC to the cooperative unfolding of the native 3WJ. The refolding FDC shows two kinds of events: the reversible folding to an intermediate, denoted as I_N, followed by the cooperative folding to N.

Less frequently ($\simeq$10% of the times), we observe the unfolding of 2HM (rightmost curves in Fig. 3 *B* and *C*). A shoulder in the FDCs is observed around $f \sim 11$ pN, followed by a marked force rip at $\sim$ 15 pN. As we explain below, these two events are identified as the non-cooperative and cooperative unfolding of H_1^M and H_2^M, respectively (Fig. 1 *B*, right). The same patterns for the unfolding and folding FDCs are observed in magnesium and sodium, showing that the secondary structures that are formed (3WJ and 2HM) are the same for the two salt conditions (Fig. 1 *B*). The molecular free energy landscape (FEL) of the secondary structures for N and M as predicted by Mfold and the elastic response of the ssRNA were calculated at 1 M NaCl and at different forces and are shown in Fig. 4 *A* and *B* (Section 2 in Supporting material). The FELs present local minima that correspond to intermediates of N and M folding reactions detected in experiments (see below). In Fig. 4 *C* and *D*, we show the N and M folding reaction pathways based on the FEL.

Folding-unfolding kinetics was investigated in hopping and pulling experiments (Materials and methods). In

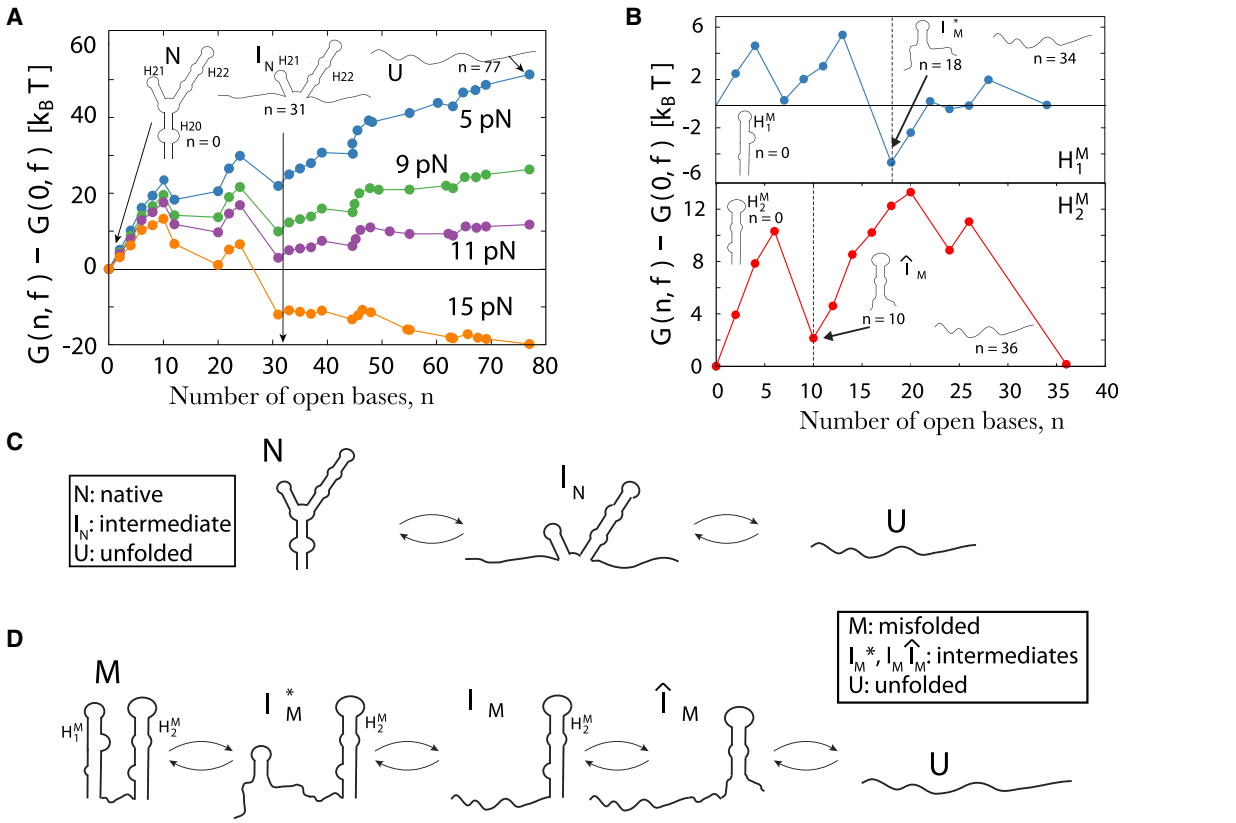

FIGURE 4 Folding energy landscapes (FELs) and folding-unfolding (F-U) pathways for the N and M structures. (*A* and *B*) FELs (298 K, 1 M NaCl) at different forces for N and for the hairpins forming M at their coexistence forces (11.5 pN for H_1^M and 13 pN for H_2^M). Note the higher barrier for H_2^M ($\approx 12 k_B T$). The folded, unfolded, and intermediate structures are schematically depicted. Points in the FELs versus the number of open bases are not always regularly spaced, resulting in gaps between contiguous configurations. For instance, opening the seventh base of the 3WJ yields a six-base avalanche due to the release of the internal loop. F-U reaction pathways for (*C*) N (upper) and (*D*) M (lower). They show the main intermediates detected in experiments that correspond to the local minima in the FELs shown in (*A*) and (*B*). To see this figure in color, go online.

hopping experiments, the control parameter (i.e., the distance between the trap and the micropipette, labeled as "Distance" in Fig. 3 *A*) is kept fixed while the RNA samples the equilibrium state. Force-dependent kinetic rates are measured from the lifetimes of the states at different forces. In pulling experiments, kinetics is obtained from unfolding and folding force distributions [56,57]. Next, we study the folding/unfolding kinetics of the misfolded 2HM and the native 3WJ.

Misfolded structure: Equivalent sodium concentration

We have used the misfolded structure (M $\equiv$ 2HM) to verify that roughly 100 times of sodium is equivalent to the magnesium concentration, as predicted by RNA unzipping studies [25,30]. Mechanical unfolding of M proceeds in two steps: first H_1^M reversibly unfolds at $f \sim 11$pN, followed by the unraveling of H_2^M at $f \sim 15$ pN (ellipses in Fig. 5 *A*). The two distinct unfolding steps are related to specific features of the FEL of each hairpin as shown in Fig. 4 *B*: while the FEL of H_1^M is nearly flat, the FEL of H_2^M has large kinetic barriers on the order of 10 $k_B T$. The unfolding of H_2^M is expected to be more cooperative than H_1^M.

In Fig. 5 *B* we show rupture force distributions of H_2^M in magnesium and sodium. The state where H_1^M is unfolded and H_2^M is folded is an intermediate between M and U that we will denote as I_M. Bell-Evans kinetic rates (Section 3 in Supporting material) for transitions $I_M \leftrightarrow$ U are shown in Fig. 5 *B* (inset) and the FEL parameters are reported in Table 1. These are the same for magnesium and sodium (within errors). The sum of the two distances to the transition state, $x^{\dagger}_{I_M - U} + x^{\dagger}_{U - I_M} \approx 8$ nm (~22 bases) is $\simeq 60\%$ of the expected molecular extension released in H_2^M unfolding (i.e., 36 bases or 13 nm, red FEL in Fig. 4 *B*). This suggests that the first $\sim$ 10 bases in H_2^M are already unfolded consistently with the FEL minimum at $n = 10$ in H_2^M (Fig. 4 *B*, red FEL). This misfolded intermediate is named $\hat{I}_M$. The schematic of the folding reaction pathway for M showing the different misfolding intermediates is plotted in Fig. 4 *D*.

We also studied the unfolding/folding kinetics of M $\leftrightarrow I_M$ by monitoring the non-cooperative transitions between H_1^M and M in hopping experiments. Kinetic rates and the results

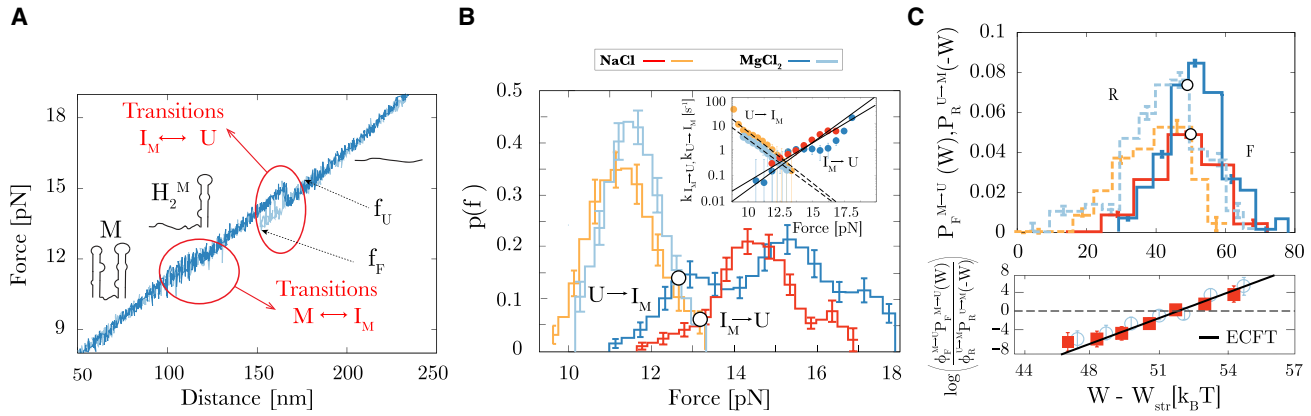

FIGURE 5 Free energy and kinetics of the misfolded 2HM. (*A*) A typical FDC for M showing the unfolding and folding in dark blue and light blue, respectively. Regions where transitions $I_M \leftrightarrow U$ and $M \leftrightarrow I_M$ are observed are encircled in red. The structures corresponding to M, I_M, and U are schematically shown in the figure. The rupture and folding forces for I_M, denoted as f_U and f_F respectively, are indicated with dotted black arrows. (*B*) Rupture and folding force distributions for I_M and Bell-Evans kinetics (inset) in magnesium (light and dark blue) and sodium (red and orange). Dark (light) colors correspond to unfolding (folding) forces. Errors were computed with bootstrapping. Pulling speed equals to 200 nm/s. Circles highlight the coexistence force (crossing point of the unfolding and folding distributions). (*C*) Partial work distributions for $M \leftrightarrow U$ for the F (unfolding) and R (folding) processes obtained in magnesium and sodium and test of the validity of the ECFT (lower). Same color code as in (*B*). Pulling speed equals to 200 nm/s. Error bars in the histograms have been calculated using the bootstrap method. The intersection between forward and reversed distributions correspond to the free energy difference value estimated as described in Ref. [58]. To see this figure in color, go online.

of the continuous effective barrier analysis (CEBA) [57,59] are shown in Fig. S2 (Supporting material) for sodium only. In magnesium, the native 3WJ is rescued (see below) and hopping $M \leftrightarrow I_M$ is unstable, making the comparison between magnesium and sodium difficult.

We measured the free energy of folding of M in magnesium and sodium by using the ECFT, Eq. 5 (Materials and Methods). The ECFT is an extension of CFT [46,52] useful to determine free energies of non-native states [53,54]. We applied Eq. 5 with $A \equiv M, B \equiv U$. In Fig. 5 *C*, we show the partial forward ($P_F^{M\to U}(W)$) and partial reverse ($P_R^{U\to M}(-W)$) work distributions conditioned to start from M and U along the F and R processes, respectively. The validity of the ECFT is shown in Fig. 5 *C* (bottom). There we plot the logarithm of the ratio of the forward and reverse work distributions (in k_BT units) corrected by the fraction of folding trajectories $\varphi_R^{U\to M}$ ending in *M* during the R process. Note that in Eq. 5 the fraction of unfolding trajectories $\varphi_F^{M\to U} = 1$ as the molecule is always unfolded at the end of the F process. As predicted by Eq. 5, the slope is ~ 1 (black solid line). Stretching energy contributions (W_{str}) to the experimental setup (i.e., bead displacement, handles, and ssRNA) have been subtracted from the total free energy ΔG_{MU} (see Section 4 in Supporting material for details). The free energies obtained, ΔG^0_{MU}, are referenced to the random coil state at zero force. We obtain $\Delta G^0_{MU} = 52(4)k_BT = 31(2)$ kcal/mol in magnesium and $\Delta G^0_{NU} = 54(4)k_BT = 32(2)$ kcal/mol in sodium (Table 2). Therefore, we have verified that the folding free energy of M is the same in Mg^{2+} and Na^+. This result has two implications. First and foremost, it confirms that the non-specific binding energy of magnesium and sodium ions is the same at the chosen experimental conditions. Second, since M does not form the Mg^{2+} binding site (the junction), there is no specific binding energy of Mg^{2+} to M. Finally, the sodium equivalent extends also to kinetics: the unfolding and folding kinetic rates $k_{I_M\to U}, k_{I_U\to M}$ are roughly equal in magnesium and sodium. The same holds for the kinetics between I_N and U (see next section). Therefore, in a first approximation, the non-specific binding of 1 M NaCl to RNA is equivalent to 10 mM $MgCl_2$ at the level of thermodynamics [30] but also at the level of kinetics.

Native RNA 3WJ structure

Unfolding of the 3WJ is observed as a force rip at the unfolding force $f_U \sim 15 - 24$, for the transition $N \to U$, measured in the native (N) branch (FDC shown in Fig. 6 *A* in sodium). Upon refolding, the FDC in the unfolded (U) branch shows a shoulder at $f \sim 12$–13 pN, for the transition $U \to I_N$, from U to a native-folding intermediate I_N. This is followed by the folding transition $I_N \to N$ at a force (f_F) measured in the U branch (Fig. 6 *A*). The presence of I_N is supported by the FEL (Fig. 4 *A*). At $f \sim 11$ pN, the FEL has a minimum when $\simeq 31$ bases are unzipped, which we identify as the intermediate I_N observed in the FDCs. Note that the FEL shown in Fig. 4 *A* must change upon Mg^{2+} binding [60]. The schematics of the folding reaction pathway for N is shown in Fig. 4 *C*.

Rupture ($N \to U$) and folding ($I_N \to N$) force distributions are shown in Fig. 6 *B* for magnesium and sodium. Kinetic rates $k_{N\to U}$ and $k_{I_N\to N}$ were extracted as described in Eqs. S13 and S14 in the Supporting material. These have been fitted to the Bell-Evans model (Section 3 in the Supporting

TABLE 1 Fitting parameters of the kinetic rates for 2HM and the 3WJ to the Bell-Evans model

2HM	$x^{\dagger}_{I_M-U}$ (nm)	$x^{\dagger}_{U-I_M}$ (nm)	ΔG_{I_MU} (k_BT)	f_c (pN)
10 mM $MgCl_2$	3.4 (2)	4.7 (1)	26 (1)	13.1 (6)
1 M NaCl	3.3 (5)	4.7 (2)	25 (2)	12.6 (4)
3WJ	$x^{\dagger}_{N-U}$ (nm)	$x^{\dagger}_{I_N-N}$ (nm)	$x^{\dagger}_{I_N-U}$ (nm)	$x^{\dagger}_{U-I_N}$ (nm)
10 mM $MgCl_2$	1 (1)	3 (1)	9.8 (5)	9.1 (5)
1 M NaCl	3.0 (7)	4.2 (4)	6 (1)	11 (1)

Parameters are obtained by fitting the data shown in the insets of Figs. 5 *B* and 6 *B* to Eqs. S9 and S10 in the Supporting material. Results are obtained by averaging parameters over four different pulling speeds (50, 100, 200, and 500 nm/s), and six different molecules per speed.

TABLE 2 Experimental measurement of ΔG^0_{NU} and ΔG^0_{MU} at $T = 298K$

	ΔG^0_{NU} (k_BT)	ΔG^0_{NU} (kcal/mol)	ΔG^0_{MU} (k_BT)	ΔG^0_{MU} (kcal/mol)
10 mM $MgCl_2$	87(4)	52(3)	52(4)	31(2)
1 M NaCl	70(4)	42(3)	54(4)	32(2)

Free energies have been obtained using the ECFT (Eq. 5). Error bars contain statistical and systematic errors. Experiments were performed at four different pulling speeds (50, 100, 200, and 500 nm/s) for six different molecules (stretching contributions are reported in Table S1).

material) with transition state distances from states N and I_N, $x^{\dagger}_{N-U}$ and $x^{\dagger}_{I_N-N}$ as fitting parameters (continuous and dashed lines in Fig. 6 *B*, inset). The parameters are reported in Table 1. Notice that I_N is only observed during the refolding process (lower encircled regions in Fig. 6 *A*); therefore, we cannot directly measure $x_{N-I^{\dagger}_N}$ from the FDCs.

The force jump N → U (Fig. 6 *A*) corresponds to the release of 73(4) nucleotides (consistent with the 77 nucleotides of the 3WJ). The force jump $I_N \rightarrow$ N gives 31(3) absorbed nucleotides, proving that I_N corresponds to the native-folding intermediate depicted in Fig. 4 *A–C*, where helices H21 and H22 are formed but the stem H20 is not (Section 1 in Supporting material).

We further studied I_N by performing hopping experiments in the region where multiple transitions $I_N \leftrightarrow$ U occur (Fig. 6 *C*, top). Force distributions show two maxima corresponding to states I_N and U that can be fitted to the sum of two Gaussians (Fig. 6 *C*, top right). The difference of the Gaussian centers gives 42(4) and 40(3) for the number of released nucleotides in magnesium and sodium, respectively. This number adds to the previously obtained 31(3) nucleotides for the $I_N \rightarrow$ N transition giving the expected 73(4) total number of nucleotides of the 3WJ. Kinetic rates $k_{I_N \rightarrow U}$ and $k_{U \rightarrow I_N}$ are obtained by measuring the lifetime of each state at different forces (Fig. 6 *C*, bottom) and fitted to the Bell-Evans model (Section 3 in the Supporting material). This permits us to extract the distances from I_N and U to the transition state, $x^{\dagger}_{I_N-U}$ and $x^{\dagger}_{U-I_N}$ (Table 1). The numbers of released nucleotides and transition state distances agree with the FEL predictions shown in Fig. 4 *A*. The folding free energy of I_N can be obtained using the continuous effective barrier analysis (CEBA) [57,59] (Fig. S3 and Section 5 in the Supporting material). We obtain $\Delta G^0_{I_NU} = 58(5)\, k_BT$ and $49(4)\, k_BT$ for magnesium and sodium, respectively. This shows that magnesium stabilizes I_N with respect to sodium by almost $10\, k_BT$.

As we did for M in Fig. 5 *C*, we also measured the free energy of folding of N in magnesium and sodium using the ECFT Eq. 5 (Materials and Methods). In Fig. 6 *D* (top) we show the partial forward ($P_F^{N \rightarrow U}(W)$) and partial reverse ($P_R^{U \rightarrow N}(-W)$) work distributions conditioned to start from N and U at the beginning of the F and R processes, respectively. The validity of the ECFT is shown in Fig. 6 *D* (bottom), where we plot the logarithm of the ratio of the forward and reverse work distributions multiplied by the fraction of native folding trajectories $\varphi_R^{U \rightarrow N}$, as a function of work in k_BT units (notice that, as in the previous case for *M*, $\varphi_F^{N \rightarrow U} = 1$). Again, the slope is close to 1 (solid lines in Fig. 6 *D*, bottom). Stretching energy contributions (W_{str}) to the experimental setup (i.e., bead displacement, handles, and ssRNA) have been subtracted to the total free energy ΔG_{NU} (Section 4 in the Supporting material). We obtain $\Delta G^0_{NU} = 87(4)\, k_BT$ =52(3) kcal/mol in magnesium and $\Delta G^0_{NU} = 70(4)\, k_BT$ =42(3) kcal/mol in sodium, giving a difference of $\Delta\Delta G^0_{NU} = 17\, k_BT = 10$ kcal/mol for the stabilizing effect of magnesium (Table 2).

Specific Mg^{2+} binding energy to the 3WJ

We have seen that Mg^{2+} stabilizes the 3WJ by 10 kcal/mol, compared with its equivalent sodium. This difference is thermodynamic and has been obtained by applying the ECFT to irreversible pulling experiments. In fact, the misfolded structure forms about 10% of the time after releasing the force. If N and M structures coexisted in equilibrium, such frequency would indicate a free energy difference of about $-k_BT \log(0.1) \simeq 2.3\, k_BT$. However, the free energy difference is much larger ($\simeq 17\, k_BT = 10$ kcal/mol), meaning that M kinetically traps the RNA during folding.

In Table 2 we report the measured values for ΔG^0_{NU}, ΔG^0_{MU}. The free energies obtained in 1 M NaCl for N and M are consistent with Mfold predictions: $\Delta G^0_{NU} = 67\, k_BT = 40$ kcal/mol and $\Delta G^0_{MU} = 50\, k_BT = 30$ kcal/mol.

Since the folding free energy of M is the same in Mg^{2+} and Na^+, this shows that we are in equivalent salt conditions, as expected [30]. Therefore, the difference in folding free energy of N in the two conditions must come from Mg^{2+}-specific binding. Previous studies have shown that, in the presence of S15 protein, three Mg^{2+} bind to the 3WJ at the junction [34,41] (see Fig. 2). Without protein, Mg^{2+} still binds to the junction, inducing a conformational change. The difference in energies is $\Delta\Delta G_{NU} = \Delta G^{MgCl_2}_{NU} - \Delta G^{NaCl}_{NU} = 17(5) k_BT = 10(3)$

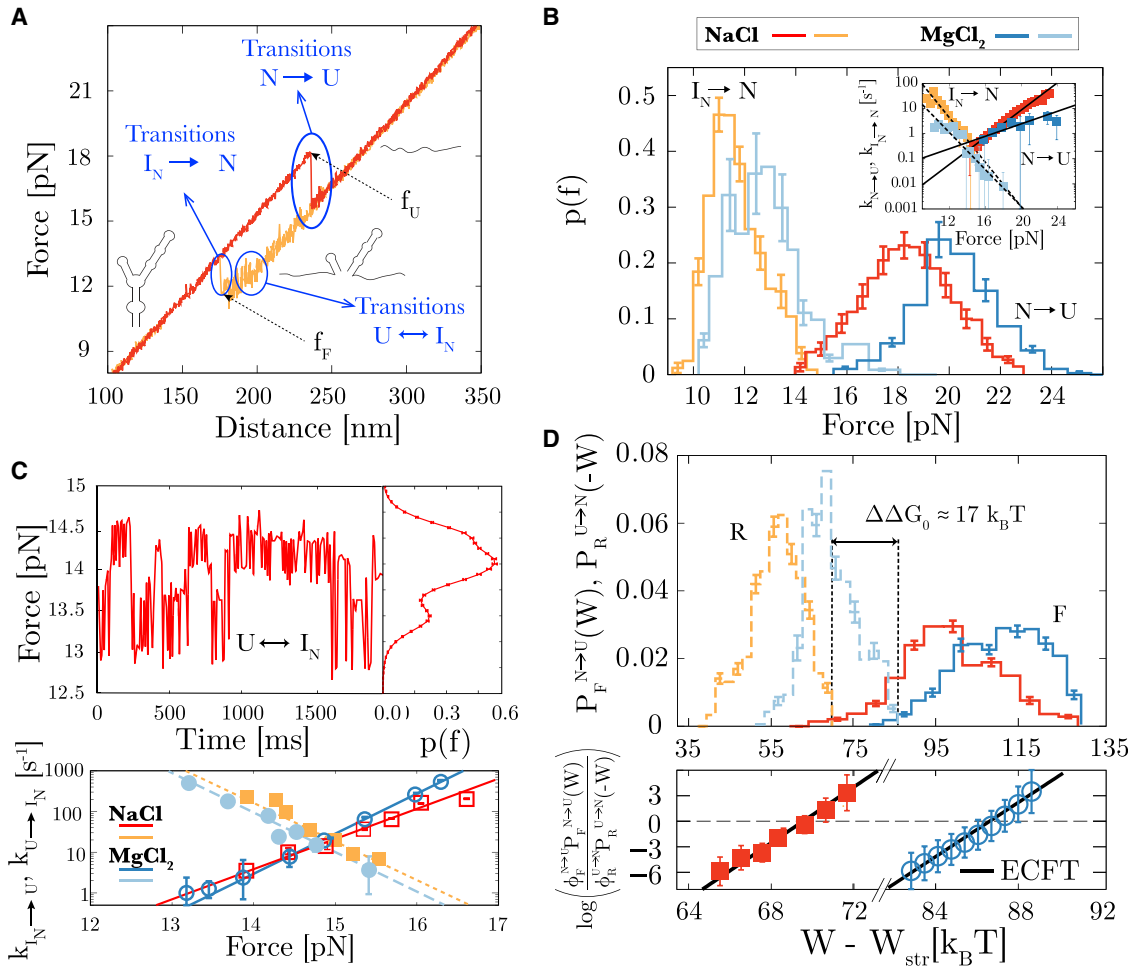

FIGURE 6 Free energy and unfolding-folding kinetics of the native 3WJ. (*A*) A typical FDC for N showing the unfolding and folding in red and orange, respectively. Regions where transitions $I_N \leftrightarrow N$ and $U \leftrightarrow I_N$ are observed are encircled in blue. The structures corresponding to N, I_N, and U are schematically shown in the figure. The rupture and folding forces for N, denoted as f_U and f_F respectively, are indicated with dotted black arrows. (*B*) Rupture and folding force distributions, $N \rightarrow U$ and $I_N \rightarrow N$ respectively, and kinetic rates versus force (insets) in magnesium (dark and light blue) and sodium (red and orange). Dark (light) colors correspond to unfolding (folding) forces. Black lines are predictions by the Bell-Evans model. Errors were computed with bootstrapping. Pulling speed is 200 nm/s for both cases. (*C*) (Top) Hopping trace $I_N \leftrightarrow U$ and force histograms in sodium (right). (Bottom) Kinetic rates and Bell-Evans model prediction (straight lines) in magnesium (dark and light blue) and sodium (red and orange). Empty (filled) symbols correspond to $k_{I_N \rightarrow U}$ ($k_{U \rightarrow I_N}$). (*D*) Partial work distributions for $N \leftrightarrow U$ for the F (unfolding) and R (folding) processes obtained in magnesium and sodium (top) and test of the validity of the ECFT (bottom). Same color code as in (*B*). Pulling speed equals to 200 nm/s. To see this figure in color, go online.

kcal/mol. For three Mg^{2+} ions, this yields an average binding energy of 6(2) k_BT or 4(1) kcal/mol per Mg^{2+} ion.

Rescue of the 3WJ

Upon releasing the force, one can find conditions where the RNA hops between M and its intermediate I_M. A typical hopping trace in magnesium is shown in Fig. 7 *A*. During the first ∼25 s (horizontal red arrow marked as τ_R), the RNA executes fast transitions between I_M and M (force levels indicated as dashed and dotted lines, respectively). At the time $\tau_R \sim 25s$, hopping $I_M \leftrightarrow M$ stops with a sudden force jump to N. Thereafter the molecule does not hop back to M anymore (after τ_R in Fig. 7 *A*). Folding to N at τ_R is preceded by a fast event where M unfolds and the force drops to a minimum value (∼ 11.8 pN, bottom continuous line) in a process known as rescue [61].

In a rescue experiment, a refolding process is implemented starting from U. The force is monitored until the cooperative folding of the misfolded hairpin H_2^M is observed. Fig. 5 *A* shows a typical refolding curve (light blue) where H_2^M is formed first at ∼ 14 pN (upper red circle in Fig. 5 *A*). Below ∼ 14 pN, the molecule enters I_M and hopping is observed between M and I_M (lower red circle in Fig. 5 *A*). At this point, the releasing process stops and the trap position is kept fixed while force is measured (rescue trace in Fig. 7 *A*). The duration of this hopping trace defines the rescue time τ_R (horizontal red arrow in Fig. 7 *A*). We measured a total of about 50 rescue events in magnesium and sodium at different force conditions. Rescue times

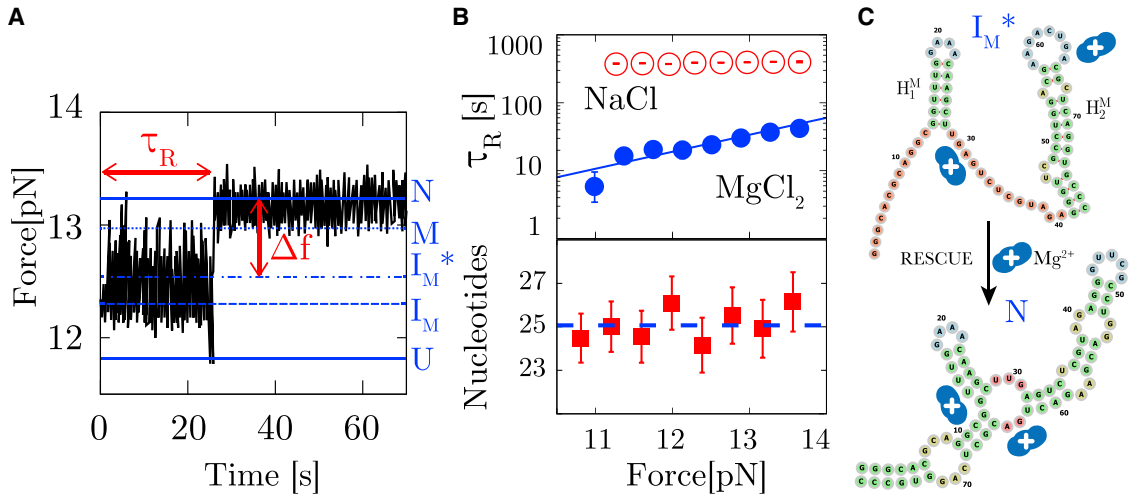

FIGURE 7 Rescue of the native 3WJ. (*A*) A typical force-time rescue trace in magnesium. The RNA initially hops between M and I_M (between 0 and $\tau_R \sim 25$ s in the trace). After τ_R, the molecule unfolds to U and next folds to N. The force jump between the rescuing intermediate $I_M^\star$ and N is shown as Δf (see text). On the right vertical axis we indicate the states corresponding to the different force levels (horizontal blue lines). (*B*) (Top) Rescue time as a function of force (top) in magnesium (filled symbols) and sodium (empty symbols). The Bell-Evans fit is shown as a continuous line for magnesium. (Bottom) The rescued number of nucleotides (between $I_M^\star$ and N given by Δf) versus force. Error bars are statistical errors measured over six molecules in magnesium. The dashed line corresponds to the average number of nucleotides, ~ 25. (*C*) Hypothesized long-range rescue mechanism where the presence of Mg^{2+} ions (shown as a blue cloud of a positive charge) bring together distant nucleotides in 2HM. The blue clouds do not indicate specific binding. Instead, they schematically represent long-range attractive interactions that rescue the native structure. To see this figure in color, go online.

(Fig. 7 *B*, top) are in the scale of 10 s in magnesium (blue circles) and tens of minutes in sodium (red circles), showing the rescuing effect of Mg^{2+}. Interestingly, the average rescue time increases with force in magnesium (blue circles in Fig. 7 *B*, top) whereas for sodium it remains constant. This fact shows that Mg^{2+}-induced rescue is an activated-diffusive process over a force-dependent kinetic barrier, whereas for sodium rescue is diffusion limited (with a force-independent barrier). These distinct dependencies suggest that there is transition state mediating the rescue process in magnesium. In contrast, in sodium, such a mediating transition state is not observed and rescue occurs by thermal diffusion alone.

Rescue implies a positive force jump that we indicate in Fig. 7 *A* by Δf, from a given force value within the hopping trace $I_M \leftrightarrow M$ to the force level in N (continuous blue line in Fig. 7 *A*, top). The force jump Δf implies the absorption of a molecular extension equal to 12(1) nm in the range [11–14 pN] for sodium and magnesium. Using the worm-like chain model for RNA [25] we have converted the extension into number of nucleotides (Fig. 7 *B*, bottom). The number of nucleotides (~ 25, blue dashed line in Fig. 7 *B*, bottom) is force independent and compatible with an initial conformation previous to rescue in which hairpin H_2^M is completely formed, whereas hairpin H_1^M is only partly formed by the hybridization of the 6 bp preceding the GAAA loop (Fig. 7 *C*, top). We denote this conformation by $I_M^\star$ (shown in Fig. 7 *A* as a dashed-dotted blue line). $I_M^\star$ corresponds to a second intermediate between M and I_M, which is predicted by the FEL of hairpin H_1^M as a minimum located at $n \sim 18$ in Fig. 4 *B* (top). We hypothesize a long-range rescue mechanism where the two positive charges of Mg^{2+}, assisted by thermal fluctuations, bring together the two distant regions of the misfolded RNA structure (blue positive charged clouds in Fig. 7 *C*, top) required to form the native junction. The regions are the internal loop of H_1^M (around positions 28–30) and the loop of H_1^M (around positions 64–66). These regions are observed to contain specific magnesium ions in the crystallographic structures of the native 3WJ, as shown in Fig. 2. The close-up of these regions is stabilized by the positive Mg^{2+} charges that facilitate the formation of the junction in a thermally activated process (Fig. 7 *C*, bottom).

The force dependence of the rescue time for magnesium can be fitted to the Bell-Evans model giving a distance to the transition state of $x^{\dagger\dagger} \simeq 2$ nm (continuous blue line in Fig. 7 *B*, top). This value is about half the distance between the internal loop of H_1^M (around position 30) and the end loop of H_2^M (around position 64), supporting the fact that rescue in magnesium is a thermally activated process. In sodium, such force dependence is not observed, because the rescue pathway is diffusion limited without involving long-range attractive interactions between divalent charges in specific binding sites.

DISCUSSION

We have introduced a single-molecule method to determine the specific energy contribution of Mg^{2+} binding to tertiary RNAs. The method requires the knowledge of the equivalent amount of sodium that binds non-specifically to the native RNA structure. The sodium equivalent can be determined using the 1/100 empirical salt rule reported in previous studies

[25,27,28], and that has been recently demonstrated at the single-molecule level [30]. We applied the method to the highly conserved site of the 16S rRNA from *E. coli* that contains a 3WJ acting as the binding site of three Mg^{2+}. We measured the free energies of the 3WJ at 10 mM $MgCl_2$ and at its sodium equivalent, 1 M NaCl. We find a stabilization free energy due to Mg^{2+} binding of 10(3) kcal/mol at 298K. For three Mg^{2+} binding to the 3WJ, this amounts to an average of $\sim$ 3.5 kcal/mol per cation. It is interesting to compare this number with theoretical predictions of Mg^{2+} site binding in tertiary RNAs, such as the 58-nucleotide fragment from the *E. coli* 23S rRNA subunit, which gives 4.8 kcal/mol [22], or the overall stabilization due to Mg^{2+} of an A-riboswitch, 9.8 kcal/mol [62]. Estimations of Mg^{2+} binding energies based on chemical shift deviations in 2D-NMR spectra fall in the range of 2–3 kcal/mol [63].

Our method to determine the specific Mg^{2+} binding energy relies on two assumptions: the empirical salt rule (i.e., there is a sodium equivalent for the non-specific binding free energy in magnesium, Eq. 1), and the additivity rule (i.e., specific and non-specific energy contributions in magnesium are additive, Eq. 2). The validity of the empirical rule has been disputed on the basis of measurements of the fraction of dissociated ions [64,65] rather than the direct free energy measurements in single-molecule studies [30].

The empirical salt rule has been further verified using a misfolded structure that does not contain Mg^{2+}-specific binding sites. In fact, the studied RNA forms a misfolded structure (2HM) of lower thermodynamic stability (by $\sim$16 k_BT) with respect to the native 3WJ (standard sodium conditions). 2HM consists of two serially connected hairpins, as predicted by the Mfold algorithm for RNA secondary structures. A dynamic force spectroscopy study of the thermodynamics and kinetics of M shows that 1 M NaCl is approximately the equivalent sodium concentration of 10 mM $MgCl_2$, consistent with the above-mentioned 1/100 empirical rule. Despite the apparent generality of the empirical salt rule, it is convenient to use M as a reference state to calibrate the magnitude of the non-specific binding energy. It remains open to ascertain the reach of this rule and how it depends on temperature and salt type.

The additivity rule Eq. 2 might be further confirmed by magnesium titration experiments. In this case, both (non-specific and specific) energy contributions might depend differently on salt. While corrections to the non-specific salt energy contribution would be consistent with activity theories of diluted ionic solutions [25], corrections to the specific energy term should follow the law of mass action [66].

We have also found that Mg^{2+} does not only stabilize the native 3WJ; it also rescues it from the misfolded 2HM in timescales of seconds. Mg^{2+} specifically recognizes a highly negatively charged binding pocket in the junction triggering the rescue of the 3WJ by bringing together distant RNA nucleotides in 2HM. Despite the substantial energy cost of dehydrating the ion, the large electrostatic attraction in the binding pocket makes the 3WJ energetically favorable. Interestingly, rescue kinetics are very different in sodium and magnesium. While the rescue time is force-independent in sodium, it grows with force in magnesium, indicative of a transition state along the rescue pathway. The transition state is produced by the two positive charges of Mg^{2+}. Their affinity to the negatively charged phosphates facilitates bringing together distant nucleotides in M against the stretching force, promoting the formation of the native 3WJ. In sodium, the effect is absent, causing rescue times to be 10–100 times larger. The hypothesized long-range rescue effect in magnesium resonates with the mechanisms of compaction observed in ssRNA viruses in the self-assembly of viral particles (virions) [67].

The generality of the approach proposed in this work should make it also possible to derive enthalpies and entropies of Mg^{2+} binding [68] by performing pulling experiments at different temperatures [69,70]. The accurate determination of salt corrections, enthalpies, and entropies is left for future work. Finally, it would be interesting to apply the method to other cases, such as the ribosomal subunit from *Haloarcula marismortui* [71], the ribozyme from the *Tetrahymena thermophila* group I intron [27,72–74], the S15-expressing mRNA pseudoknot from *E. coli* [75], the bacterial GTP-ase center rRNA [76], and, in general, other magnesium-binding architectures [77] available in several databases (e.g., MeRNA [78] and MINAS [79]). Extension of the approach should also consider the case of different types of cations (e.g., K^+, Na^+, Mg^{++}, Ca^{++}, or even supramolecular helicates [80]). Interestingly, the methodology presented in this work can also present applications in drug design. The knowledge of the binding energy of a particular cation site can be used to choose an organic molecule or a fragment of a molecule to replace the metal ion. For instance, TPP riboswitch has two Mg^{2+} cations mediating interactions of TPP with RNA. Replacing these ions with other molecules could potentially lead to the development of a drug distinct from natural ligand TPP. Competitive binding effects (at sufficiently high concentrations) between monovalent and divalent binding cations (where energy contributions are not additive anymore) could also be investigated. Finally, the method should be extended to RNA-binding proteins [81,82]. This may require applying nonequilibrium work relations for ligand binding [66,83] to separate multiple energy contributions coming from non-specific and specific Mg^{2+} and protein binding to RNA.

SUPPORTING MATERIAL

Supporting material can be found online at https://doi.org/10.1016/j.bpj.2022.07.020.

AUTHOR CONTRIBUTIONS

A.M.M. performed the experiments and the data analysis. I.P. prepared the RNA substrate. C.B., M.M., and F.R. designed experiments and wrote the paper.

ACKNOWLEDGMENTS

This paper is written in memoriam of our great mentor and friend Nacho Tinoco with whom we started a fruitful collaboration on this topic many years ago. We are grateful to Eric Westhof and Alexander Serganov for useful discussions and a critical reading of the manuscript. We are indebted to E. Beltran and C. Verdia for their contribution at the initial stages of this work. Funding: A.M.M. and F.R. have been supported by the Spanish Research Council grants (FIS2016-80458-P, PID2019-111148GB-100). F.R. acknowledges the Catalan ICREA Academia Prizes 2013 and 2018. M.M. acknowledges support from EU Horizon 2020 grant no. 687089 and the Spanish Ramon y Cajal programme of MICINN. C.B. has been supported by the National Institutes of Health grant R01GM032543. C.B. is an investigator with the Howard Hughes Medical Institute.

DECLARATION OF INTERESTS

The authors declare no competing interests.

REFERENCES

1. Wright, M. R. 2007. An Introduction to Aqueous Electrolyte Solutions. John Wiley & Sons.
2. Sinden, R. R. 2012. DNA Structure and Function. Elsevier.
3. Feig, A. L., and O. C. Uhlenbeck. 1999. The role of metal ions in RNA biochemistry. *Cold Spring Harb. Monogr. Ser.* 37:287–320.
4. Pyle, A. M. 2002. Metal ions in the structure and function of RNA. *J. Biol. Inorg. Chem.* 7:679–690.
5. Sun, L.-Z., D. Zhang, and S.-J. Chen. 2017. Theory and modeling of RNA structure and interactions with metal ions and small molecules. *Annu. Rev. Biophys.* 46:227–246.
6. Tan, Z.-J., and S.-J. Chen. 2005. Electrostatic correlations and fluctuations for ion binding to a finite length polyelectrolyte. *J. Chem. Phys.* 122:044903.
7. Verwey, E. J. W., and J. T. G. Overbeek. 1999. Theory of the Stability of Lyophobic Colloids. Dover books on Chemistry.
8. Nguyen, H. T., N. Hori, and D. Thirumalai. 2019. Theory and simulations for RNA folding in mixtures of monovalent and divalent cations. *Proc. Natl. Acad. Sci. USA.* 116:21022–21030.
9. Auffinger, P., N. Grover, and E. Westhof. 2011. Metal ion binding to RNA. *Met. Ions Life Sci.* 9:1–35.
10. Tinoco, I., and J. S. Kieft. 1997. The ion core in RNA folding. *Nat. Struct. Biol.* 4:509–512.
11. Misra, V. K., and D. E. Draper. 1998. On the role of magnesium ions in RNA stability. *Biopolymers.* 48:113–135.
12. Draper, D. E. 2004. A guide to ions and RNA structure. *RNA.* 10:335–343.
13. Bowman, J. C., T. K. Lenz, …, L. D. Williams. 2012. Cations in charge: magnesium ions in RNA folding and catalysis. *Curr. Opin. Struct. Biol.* 22:262–272.
14. Alemán, E. A., R. Lamichhane, and D. Rueda. 2008. Exploring RNA folding one molecule at a time. *Curr. Opin. Chem. Biol.* 12:647–654.
15. Scott, W. G., J. T. Finch, and A. Klug. 1995. The crystal structure of an All-RNAhammerhead ribozyme: a proposed mechanism for RNA catalytic cleavage. *Cell.* 81:991–1002.
16. Hanna, R., and J. A. Doudna. 2000. Metal ions in ribozyme folding and catalysis. *Curr. Opin. Chem. Biol.* 4:166–170.
17. Bhaskaran, H., and R. Russell. 2007. Kinetic redistribution of native and misfolded RNAs by a dead-box chaperone. *Nature.* 449:1014–1018.
18. Ditzler, M. A., D. Rueda, …, N. G. Walter. 2008. A rugged free energy landscape separates multiple functional RNA folds throughout denaturation. *Nucleic Acids Res.* 36:7088–7099.
19. Solomatin, S. V., M. Greenfeld, …, D. Herschlag. 2010. Multiple native states reveal persistent ruggedness of an RNA folding landscape. *Nature.* 463:681–684.
20. Chastain, M., and I. Tinoco, Jr. 1991. Structural elements in RNA. *Prog. Nucleic Acid Res. Mol. Biol.* 41:131–177.
21. Tinoco, I., Jr., and C. Bustamante. 1999. How RNA folds. *J. Mol. Biol.* 293:271–281.
22. Misra, V. K., and D. E. Draper. 2001. A thermodynamic framework for mg2+ binding to RNA. *Proc. Natl. Acad. Sci. USA.* 98:12456–12461.
23. Petrov, A. S., G. Lamm, and G. R. Pack. 2005. Calculation of the binding free energy for magnesium–RNA interactions. *Biopolymers.* 77:137–154.
24. Tan, Z.-J., and S.-J. Chen. 2009. *In* Methods in Enzymology, *469*. Elsevier, pp. 465–487.
25. Bizarro, C. V., A. Alemany, and F. Ritort. 2012. Non-specific binding of na+ and mg 2+ to RNA determined by force spectroscopy methods. *Nucleic Acids Res.* 40:6922–6935.
26. Schroeder, S. J., and D. H. Turner. 2000. Factors affecting the thermodynamic stability of small asymmetric internal loops in RNA. *Biochemistry.* 39:9257–9274.
27. Heilman-Miller, S. L., D. Thirumalai, and S. A. Woodson. 2001. Role of counterion condensation in folding of the tetrahymena ribozyme. i. equilibrium stabilization by cations1. *J. Mol. Biol.* 306:1157–1166.
28. Lipfert, J., A. Y. Sim, …, S. Doniach. 2010. Dissecting electrostatic screening, specific ion binding, and ligand binding in an energetic model for glycine riboswitch folding. *RNA.* 16:708–719.
29. Manning, G. S. 1978. The molecular theory of polyelectrolyte solutions with applications to the electrostatic properties of polynucleotides. *Q. Rev. Biophys.* 11:179–246.
30. Rissone, P., C. V. Bizarro, and F. Ritort. 2022. Stem-loop formation drives RNA folding in mechanical unzipping experiments. *Proc. Natl. Acad. Sci. USA.* 119. e2025575119.
31. Martin, T. G., and H. Dietz. 2012. Magnesium-free self-assembly of multi-layer DNA objects. *Nat. Commun.* 3:1103.
32. Lescoute, A., and E. Westhof. 2006. Topology of three-way junctions in folded RNAs. *RNA.* 12:83–93.
33. Philippe, C., F. Eyermann, …, C. Ehresmann. 1993. Ribosomal protein s15 from escherichia coli modulates its own translation by trapping the ribosome on the mRNA initiation loading site. *Proc. Natl. Acad. Sci. USA.* 90:4394–4398.
34. Nikulin, A., A. Serganov, …, P. Dumas. 2000. Crystal structure of the S15-rRNA complex. *Nat. Struct. Biol.* 7:273–277.
35. Springer, M., and C. Portier. 2003. More than one way to skin a cat: translational autoregulation by ribosomal protein s15. *Nat. Struct. Biol.* 10:420–422.
36. Berglund, H., A. Rak, …, T. Härd. 1997. Solution structure of the ribosomal RNA binding protein S15 from Thermus thermophilus. *Nat. Struct. Biol.* 4:20–23.
37. Agalarov, S. C., G. Sridhar Prasad, …, J. R. Williamson. 2000. Structure of the S15, S6, S18-rRNA complex: assembly of the 30S ribosome central domain. *Science.* 288:107–113.
38. Polikanov, Y. S., S. V. Melnikov, …, T. A. Steitz. 2015. Structural insights into the role of rRNA modifications in protein synthesis and ribosome assembly. *Nat. Struct. Mol. Biol.* 22:342–344.
39. Watson, Z. L., F. R. Ward, …, J. H. D. Cate. 2020. Structure of the bacterial ribosome at 2 Å resolution. *Elife.* 9:e60482.

40. Ehresmann, C., B. Ehresmann, …, A. Serganov. 2004. Molecular mimicry in translational regulation: the case of ribosomal protein S15. *RNA Biol.* 1:66–73.

41. Serganov, A., L. Bénard, …, C. Ehresmann. 2001. Role of conserved nucleotides in building the 16 S rRNA binding site for ribosomal protein S15. *J. Mol. Biol.* 305:785–803.

42. Batey, R. T., and J. R. Williamson. 1998. Effects of polyvalent cations on the folding of an rRNA three-way junction and binding of ribosomal protein s15. *RNA.* 4:984–997.

43. Orr, J. W., P. J. Hagerman, and J. R. Williamson. 1998. Protein and mg2+-induced conformational changes in the s15 binding site of 16 s ribosomal RNA. *J. Mol. Biol.* 275:453–464.

44. Kim, H. D., G. U. Nienhaus, …, S. Chu. 2002. Mg2+-dependent conformational change of RNA studied by fluorescence correlation and fret on immobilized single molecules. *Proc. Natl. Acad. Sci. USA.* 99:4284–4289.

45. Stefan, L. R., R. Zhang, …, S. R. Holbrook. 2006. Merna: a database of metal ion binding sites in RNA structures. *Nucleic Acids Res.* 34:D131–D134.

46. Collin, D., F. Ritort, …, C. Bustamante. 2005. Verification of the crooks fluctuation theorem and recovery of RNA folding free energies. *Nature.* 437:231–234.

47. Manosas, M., I. Junier, and F. Ritort. 2008. Force-induced misfolding in RNA. *Phys. Rev. E - Stat. Nonlinear Soft Matter Phys.* 78:061925.

48. Huguet, J. M., C. V. Bizarro, …, F. Ritort. 2010. Single-molecule derivation of salt dependent base-pair free energies in DNA. *Proc. Natl. Acad. Sci. USA.* 107:15431–15436.

49. Rico-Pasto, M., I. Pastor, and F. Ritort. 2018. Force feedback effects on single molecule hopping and pulling experiments. *J. Chem. Phys.* 148:123327.

50. Forns, N., S. de Lorenzo, …, F. Ritort. 2011. Improving signal/noise resolution in single-molecule experiments using molecular constructs with short handles. *Biophys. J.* 100:1765–1774.

51. Jarzynski, C. 1997. Nonequilibrium equality for free energy differences. *Phys. Rev. Lett.* 78:2690–2693.

52. Crooks, G. E. 2000. Path-ensemble averages in systems driven far from equilibrium. *Phys. Rev. E.* 61:2361–2366.

53. Junier, I., A. Mossa, …, F. Ritort. 2009. Recovery of free energy branches in single molecule experiments. *Phys. Rev. Lett.* 102:070602.

54. Alemany, A., A. Mossa, …, F. Ritort. 2012. Experimental free-energy measurements of kinetic molecular states using fluctuation theorems. *Nat. Phys.* 8:688–694.

55. Wang, H., and H. Li. 2020. Mechanically tightening, untying and retying a protein trefoil knot by single-molecule force spectroscopy. *Chem. Sci.* 11:12512–12521.

56. Evans, E., and K. Ritchie. 1997. Dynamic strength of molecular adhesion bonds. *Biophys. J.* 72:1541–1555.

57. Alemany, A., and F. Ritort. 2017. Force-dependent folding and unfolding kinetics in DNA hairpins reveals transition-state displacements along a single pathway. *J. Phys. Chem. Lett.* 8:895–900.

58. Shirts, M. R., E. Bair, …, V. S. Pande. 2003. Equilibrium free energies from nonequilibrium measurements using maximum-likelihood methods. *Phys. Rev. Lett.* 91:140601.

59. Manosas, M., D. Collin, and F. Ritort. 2006. Force-dependent fragility in RNA hairpins. *Phys. Rev. Lett.* 96:218301.

60. Pierse, C. A., and O. K. Dudko. 2013. Kinetics and energetics of biomolecular folding and binding. *Biophys. J.* 105:L19–L22.

61. Li, P. T. X., C. Bustamante, and I. Tinoco. 2007. Real-time control of the energy landscape by force directs the folding of RNA molecules. *Proc. Natl. Acad. Sci. USA.* 104:7039–7044.

62. Leipply, D., and D. E. Draper. 2011. Effects of Mg2+ on the free energy landscape for folding a purine riboswitch RNA. *Biochemistry.* 50:2790–2799.

63. Erat, M. C., J. Coles, …, R. K. Sigel. 2012. Accurate analysis of Mg2+ binding to RNA: from classical methods to a novel iterative calculation procedure. *Coord. Chem. Rev.* 256:279–288.

64. Bai, Y., M. Greenfeld, …, D. Herschlag. 2007. Quantitative and comprehensive decomposition of the ion atmosphere around nucleic acids. *J. Am. Chem. Soc.* 129:14981–14988.

65. Lipfert, J., S. Doniach, …, D. Herschlag. 2014. Quantitative and comprehensive decomposition of the ion atmosphere around nucleic acids. *Annu. Rev. Biochem.* 83:813–841.

66. Camunas-Soler, J., A. Alemany, and F. Ritort. 2017. Experimental measurement of binding energy, selectivity, and allostery using fluctuation theorems. *Science.* 355:412–415.

67. Nicholson, B. L., and K. A. White. 2014. Functional long-range RNA–RNA interactions in positive-strand RNA viruses. *Nat. Rev. Microbiol.* 12:493–504.

68. Fiore, J. L., E. D. Holmstrom, and D. J. Nesbitt. 2012. Entropic origin of mg2+-facilitated RNA folding. *Proc. Natl. Acad. Sci. USA.* 109:2902–2907.

69. de Lorenzo, S., M. Ribezzi-Crivellari, …, F. Ritort. 2015. A temperature-jump optical trap for single-molecule manipulation. *Biophys. J.* 108:2854–2864.

70. Rico-Pasto, M., A. Zaltron, …, F. Ritort. 2022. Molten-globule like transition state of protein barnase measured with calorimetric force spectroscopy. *Proc. Natl. Acad. Sci. USA.* 119. e2112382119.

71. Klein, D. J., P. B. Moore, and T. A. Steitz. 2004. The contribution of metal ions to the structural stability of the large ribosomal subunit. *RNA.* 10:1366–1379.

72. Koculi, E., S. S. Cho, …, S. A. Woodson. 2012. Folding path of P5abc RNA involves direct coupling of secondary and tertiary structures. *Nucleic Acids Res.* 40:8011–8020.

73. Bisaria, N., M. Greenfeld, …, D. Herschlag. 2016. Kinetic and thermodynamic framework for P4-P6 RNA reveals tertiary motif modularity and modulation of the folding preferred pathway. *Proc. Natl. Acad. Sci. USA.* 113:E4956–E4965.

74. Gracia, B., H. M. Al-Hashimi, …, R. Russell. 2018. Hidden structural modules in a cooperative RNA folding transition. *Cell Rep.* 22:3240–3250.

75. Wu, Y.-J., C.-H. Wu, …, J.-D. Wen. 2014. Folding a stable RNA pseudoknot through rearrangement of two hairpin structures. *Nucleic Acids Res.* 42:4505–4515.

76. Welty, R., S. A. Pabit, …, K. B. Hall. 2018. Divalent ions tune the kinetics of a bacterial GTPase center rRNA folding transition from secondary to tertiary structure. *RNA.* 24:1828–1838.

77. Zheng, H., I. G. Shabalin, …, W. Minor. 2015. Magnesium-binding architectures in RNA crystal structures: validation, binding preferences, classification and motif detection. *Nucleic Acids Res.* 43:3789–3801.

78. Stefan, L. R., R. Zhang, …, S. R. Holbrook. 2006. Merna: a database of metal ion binding sites in RNA structures. *Nucleic Acids Res.* 34:D131–D134.

79. Schnabl, J., P. Suter, and R. K. O. Sigel. 2011. Minas—a database of metal ions in nucleic acid s. *Nucleic Acids Res.* 40:D434–D438.

80. Oleksy, A., A. Oleksi, …, M. Coll. 2006. Molecular recognition of a three-way DNA junction by a metallosupramolecular helicate. *Angew. Chem., Int. Ed. Engl.* 45:1227–1231.

81. Hentze, M. W., A. Castello, …, T. Preiss. 2018. A brave new world of RNA-binding proteins. *Nat. Rev. Mol. Cell Biol.* 19:327–341.

82. Holmqvist, E., and J. Vogel. 2018. RNA-binding proteins in bacteria. *Nat. Rev. Microbiol.* 16:601–615.

83. Koirala, D., S. Dhakal, …, H. Mao. 2011. A single-molecule platform for investigation of interactions between G-quadruplexes and small-molecule ligands. *Nat. Chem.* 3:782–787.